Representation of the Mozambique channel trough and its link to southern African rainfall in CMIP6 models

Rondrotiana Barimalala[1,2] · Rachel James[3] · Callum Munday[4] · Chris J. C. Reason[2]

Abstract

The topography of Madagascar and the strength of the Mozambique Channel Trough (MCT) modulate summer rainfall over southern Africa. A strong MCT hinders the penetration of moisture bearing easterlies from the South Indian Ocean into the mainland, thus reducing rainfall there and vice versa for weak MCT summers. Given the link between the MCT and rainfall, it is important to analyse how climate models represent the trough. Here, output from 20 models within the CMIP6 ensemble of Coupled General Circulation Models (CGCMs) are analyzed to investigate how state-of-the-art CGCMs represent the MCT and its link to southern African rainfall. Overall, the ensemble mean insignificantly underestimates the observed MCT. There is a large spread among the models, with the strength of the MCT significantly correlated with the Froude number based on the mountain height over Madagascar. In models, the vorticity tendency in the MCT area is dominated by the stretching and friction terms, whereas the vertical advection, tilting and residual terms dominate in the ERA5 reanalysis. The link between MCT and rainfall in the southern African subcontinent is missing in the models. Large rainfall biases are depicted over mainland even in models with a very strong MCT. It is found that the impacts of the MCT in the models could be masked by a complex mix of processes such as the strength of the Angola low, moisture fluxes from the Indian and South Atlantic Oceans as well as overestimated convection in the Mozambique Channel area.

Keywords Southern Africa · Mozambique channel trough · CMIP6 · Coupled climate models · Climate model evaluation

1 Introduction

Outputs from the Climate Model Intercomparison Projects (CMIP) and the Coordinated Regional Climate Downscaling Experiment (CORDEX) are often used to generate future regional climate change information. These models are assessed to be fit for purpose based on their ability to simulate the current climate state (Sushama et al. 2006; Engelbrecht et al. 2009). A common way to evaluate the performance of climate models is to compute the error with respect to the observation or through a correlation analysis (Schaller et al. 2011). These methods are routinely used by modeling centers to assess new generations of models (e.g. Gleckler et al. 2008). However, these simple comparisons do not provide any information on the mechanisms that lead to discrepancies between the models and observations, which is very crucial at regional scales. James et al. (2018) suggested that a process-based evaluation of the model outputs is needed, especially for Africa, in order to improve the representation of the continent's climate in state-of-the-art models.

Over southern Africa, climate models suffer from persistent rainfall biases and large uncertainties (Christensen et al. 2007; Dieppois et al. 2015; Lazenby et al. 2016; Munday and Washington 2017, 2018). The subcontinent is also a region where the majority of the population heavily depend on rain-fed agriculture. Reducing these rainfall biases and uncertainties are therefore crucial for the area. For the past few years, there have been increasing efforts to understand the regional processes that lead to both the biases and large uncertainties in the simulations over southern Africa (e.g. Munday and Washington 2017, 2018, 2019; Hart et al. 2019;

✉ Rondrotiana Barimalala
  ronb@norceresearch.no

1 Norwegian Research Center, Bergen, Norway

2 Department of Oceanography, University of Cape Town, Cape Town, South Africa

3 School of Geographical Sciences, University of Bristol, Bristol, UK

4 Climate Research Lab, School of Geography and the Environment, University of Oxford, Oxford, UK

Dieppois et al. 2019; James et al. 2020). These studies provide not only key information on how and where the models can be improved, but also a step towards assessing model reliability for future projections (James et al. 2018). For instance, James et al. (2020) found that the CMIP5 models reproduce the observed circulation features of the tropical-extratropical cloud bands (Hart et al. 2010, 2013), the most important summer rainfall-producing system over subtropical southern Africa, but with large inter-model differences. They suggest that a focus on tropical convection and representation of the orography could improve the simulations of cloud bands. On the other hand, Munday and Washington (2017) found that improvements in the simulation of the Angola low (AL) in the CMIP models could improve the representation of the southern African rainfall. In another study, the topography over Tanzania was found to play an important role in modulating the amount of moisture penetrating into the subcontinent. Models with high moisture transport through the Tanzanian escarpment are associated with high rainfall over the mainland (Munday and Washington 2018). Lazenby et al. (2016) analyzed the simulation of the South Indian Ocean Convergence Zone (SIOCZ) in the CMIP5 models and showed that rainfall biases over the subcontinent could be associated with excessively large low-level moisture fluxes, due to biases in the circulation over the Angola low region.

In a recent study, Barimalala et al. (2018) found that the Mozambique Channel Trough (MCT), which sits in the SIOCZ area, modulates the rainfall over the southern African subcontinent. The MCT is a low pressure area located in the Mozambique Channel (Fig. 1). It forms through the dynamical adjustment of easterly winds from the Mascarene high area to the high topography of Madagascar, while local air-sea interaction due to the relatively warm SST over the Channel may also impact its formation.

By using numerical experiments with the WRF regional climate model, the MCT was substantially weakened if the topography over Madagascar was made lower than the reality. Lowered topography in Madagascar then allows more moisture from the South Indian Ocean to penetrate into the southern African mainland, leading to increased rainfall there and a decrease in the northeastern part of Madagascar (Barimalala et al. 2018). By using output from the CMIP5 models, Munday and Washington (2017) suggests that models with a weak MCT tend to have excessive rainfall over southern Africa by strengthening the Angola low through enhanced direct moisture inflow to the subcontinent.

To our knowledge, the representation of the MCT and its characteristics in state-of-the-art climate models have not been thoroughly investigated, thus the focus of this study on analysis of output from CMIP6 (Eyring et al. 2016) models. This work is part of the Future Climate for Africa – LaunchPAD program, which aims to develop a process-based climate evaluation hub for Africa. One of the main objectives of LaunchPAD is to identify key processes that drive climate variability over Africa, and then use performance metrics associated with these mechanisms to automatically track their representation and improvement in different generations of climate models. James et al. (2018) argue that with the automation of such an assessment process, it could be possible to deliver a step change in our understanding of the behaviour of climate models.

In the following section, the data used in this work are described. The characteristics of the MCT in the CMIP6 models are then discussed in Sect. 3, followed by an investigation of the link between the MCT and southern African rainfall.

Fig. 1 Moisture flux (arrows, in $m^2.s^{-2}$) and geopotential height (shading, in m) at 850 hPa, averaged over the months of January-March in ERA5 reanalysis. White circle shows the Mozambique Channel Trough. White lines show the location of the four NE monsoon indices VN, VS, UW and UE
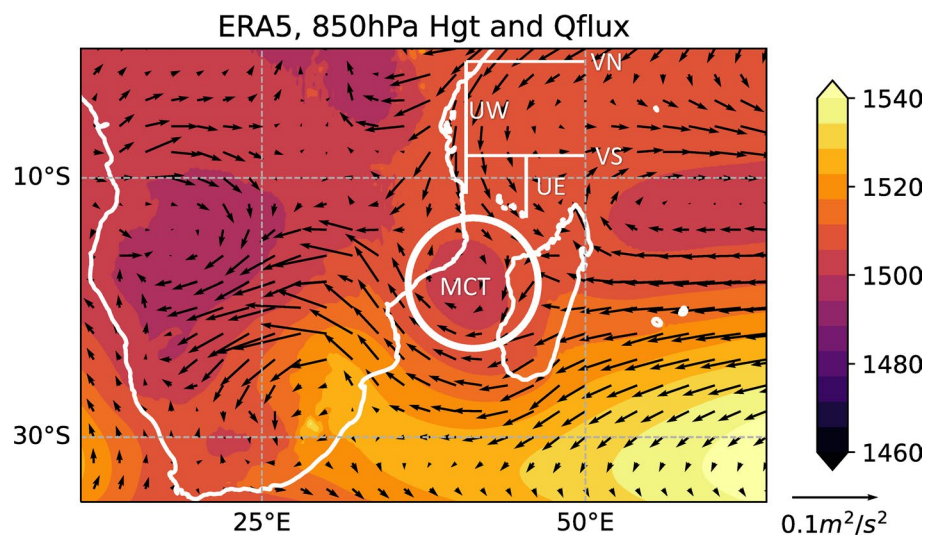
2 Data

Monthly rainfall from the Global Precipitation Climatology Project (GPCP, Alder et al. 2003) is used as observed rainfall for the period of the study (1980–2014). The GPCP data consists of a merge of rain gauge stations, satellites and sounding observations on a 2.5°×2.5° global grid. Monthly relative vorticity, geopotential height, specific humidity and wind as well as the orography from the ERA5 reanalysis data (Hersbach et al. 2020) are also used as reference for the MCT characteristics. The data has a horizontal resolution of 0.25°×0.25°.

Output from 20 models within CMIP6 are compared with the reanalysis (See Table 1). The choice of these models was based on the availability of the necessary variables from at least three ensemble members within the historical runs. For

Table 1 List of models used in the study along with their respective horizontal resolutions and the modeling groups

Model	Grid spacing	Modeling group
ACCESS-CM2	140 km	CSIRO
ACCESS-ESM1-5	140 km	CSIRO
BCC-ESM1	100 km	Beijing Climate Center
CAMS-CSM1-0	100 km	Chinese Academy of Meteorological Sciences
CanESM5	250 km	Canadian Center for Climate Modelling and Analysis
CESM2	100 km	National center for Atmospheric Research
CMCC-CM2-SR5	100 km	Centro Euro-Mediterraneo sui Cambiamenti Climatici
EC-Earth3	80 km	Consortium Europe
GFDL-ESM4	100 km	Geophysical Fluid Dynamics Laboratory
GISS-E2-1G	200 km	Goddard Institute for Space studies
GISS-E2-1H	200 km	Goddard Institute for Space studies
HadGEM3-GC31-MM	60 km	Met Office Hadley Centre
INM-CM5-0	150 km	Institute for Numerical Mathematics
IPSL-CM6A-LR	160 km	Institut Pierre-Simon Laplace
MIROC6	250 km	Consortium JAMSTEC, AORI, NIES,R-CCS
MPI-ESM1-2-HAM	170 km	HAMMOZ Consortium
MPI-ESM1-2-HR	80 km	Max Planck Institute for meteorology
MRI-ESM2-0	100 km	Meteorological Research Institute
NorESM2-LM	190 km	Norwegian Climate Center
NorESM2-MM	100 km	Norwegian Climate Center

each model, three ensemble members, re-grided to 2°×2° (for a fair comparison) are used. In all analyses, the individual members are analyzed separately, results from individual ensemble members are then averaged to be compared with the reanalysis data.

All analyses are done over the period of 1980–2014 for the months of January-March (JFM), during which the MCT is strongest, with the MCT index defined as the area average of the relative vorticity at 850 hPa over the southern Mozambique Channel (35–44°E, 16–26°S, Barimalala et al. 2018). To ensure that the choice of the period of study does not affect the MCT evaluation, given that the CMIP6 model outputs are from free-running simulations, we compared the simulated MCT climatology for 1950–2014 and 1980–2014. The differences are rather weak and insignificant (Figure S1).

An analysis of the links between the MCT, the Mascarene High (MH) pressure and the northeast (NE) monsoon flow that exists in the austral summer across the tropical western Indian Ocean is also performed. The MH index is defined as the area averaged of the mean sea level pressure (MSLP) within 40–110°E and 15–40°S. For the NE monsoon, we adopt the four indices (VN, VS, UW and UE) used in Barimalala et al. (2020) to characterize the flow from the tropical western Indian Ocean toward eastern Africa. They are defined as follows:

(i) VN, mean meridional wind averaged over 40–50°E at 1°S (Fig. 1);

(ii) VS, same as VN but farther to the south, at 9°S (Fig. 1);

(iii) UW, mean zonal wind that penetrates into southern African mainland (Fig. 1, between 1–12°S at 38°E); and.

(iv) UE, mean zonal wind over the northern Mozambique channel that flows toward Madagascar (Fig. 1, between 9–15°S at 44°E).

Statistical significance tests, using Student t-test, are performed in all differences between simulated and observed variables.

3 MCT characteristics in CMIP6

3.1 Formation of MCT

We start our analysis by examining the strength of the MCT in the climate models. Compared to ERA5, the ensemble mean of the CMIP6 models insignificantly underestimates the strength of the observed MCT (relative vorticity $= -5.46 \times 10^{-6}$ s^{-1}, Fig. 2). There is also a large spread between the models, ranging from -1.29×10^{-6} s^{-1}

Fig. 2 a MCT indices in the
CMIP6 models (blue bars),
CMIP6 models ensemble mean
(cyan) and ERA5 (red), Units in
s^{-1}. Black horizontal lines show
the spread of the members from
each model. **b** Froude number
vs MCT index in models with
Fr > 1

(a)

(b)
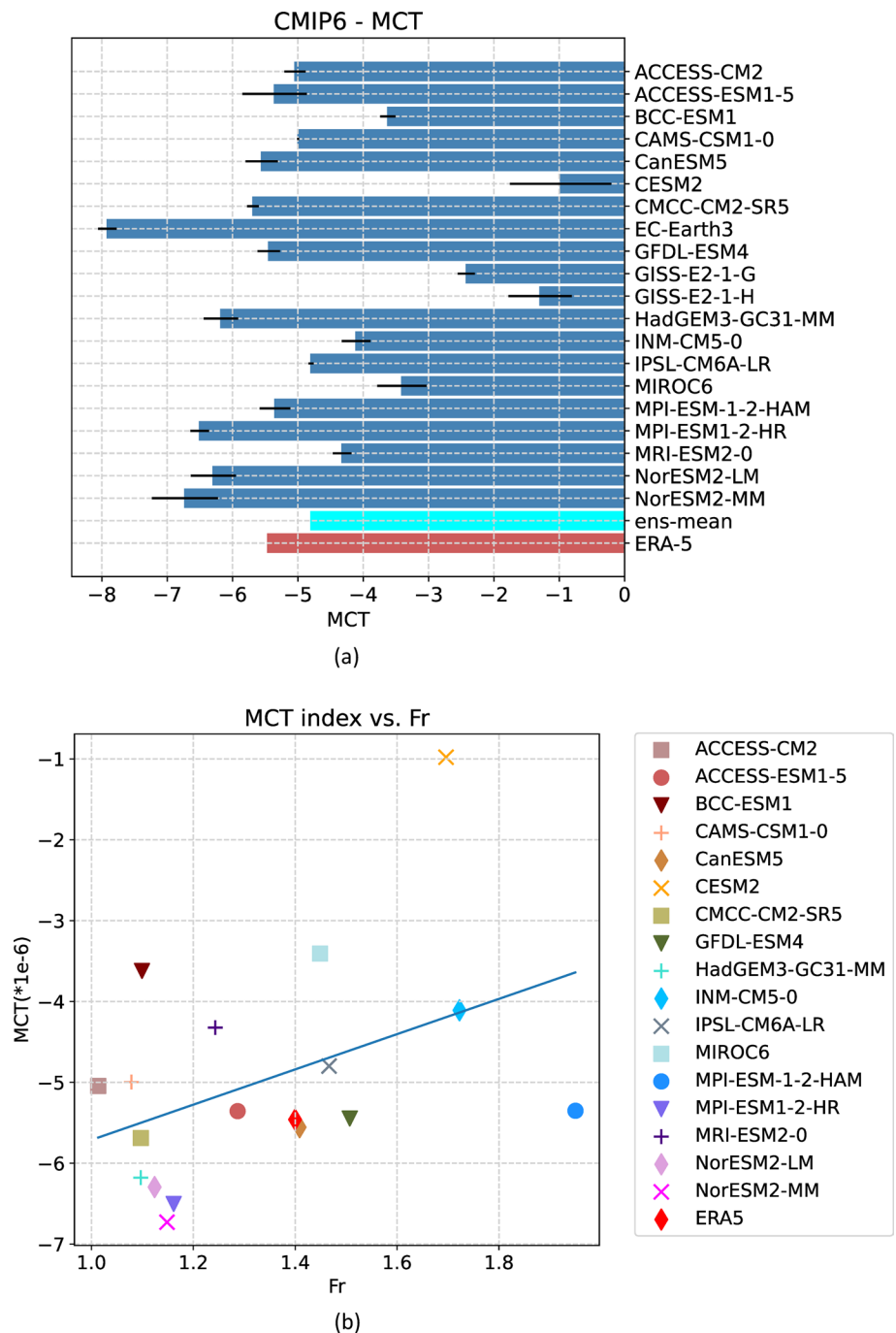
to -7.9 × 10^{-6} s^{-1}, with the CESM and two GISS models showing relatively weak MCTs and EC-Earth3 the strongest.

Barimalala et al. (2018) showed that the MCT forms through a dynamical adjustment of the easterly winds from the tropical South Indian Ocean, impacting on the high topography of Madagascar. A widely used parameter to analyze the blocking effects of topography, also adopted here, is the nondimensional Froude number (Smolarkiewicz and Rotunno 1989) defined as

$$Fr = \frac{U}{Nh}$$

where U is the mean velocity of the upstream easterlies at 850 hPa (averaged between 52-58°E and 10-26°S), N the Brunt Vaisala frequency and h the mean topography of Madagascar.

$Fr < 1$ is indicative of a completely blocked flow, whereas for $Fr > 1$, the flow could pass over the topography of Madagascar, adjust and form a lee-side trough.

Fig. 3 Latitudinal cross section of topography over Madagascar, averaged between 42-52°E. Solid lines present the CMIP6 models, and ERA5 in dashed line
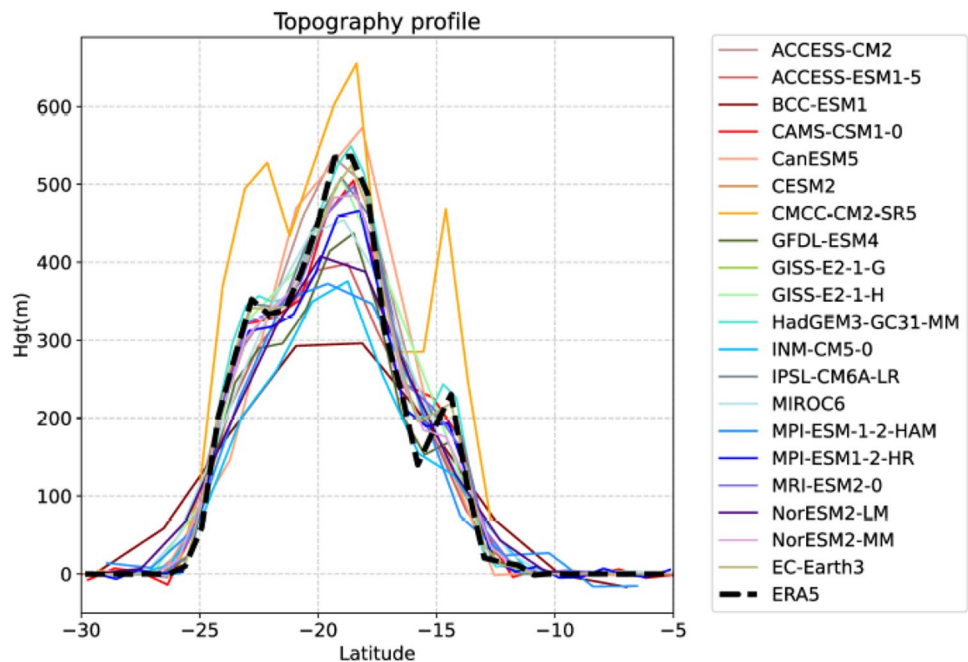

Figure 2 indicates that for climate models characterized by $Fr > 1$, there is a significant linear relationship between the strength of MCT and Fr (r = 0.45 and p-value = 0.05), in which the closer Fr to 1, the more negative the relative vorticity downstream in the Channel, and hence the stronger the MCT. In agreement with Barimalala et al. (2018), these results suggest that models with weakly blocked flow tend to have weaker MCT. On the other hand, the GISS-E2-1G model is characterized by a completely blocked flow ($Fr < 1$, Figure S2), which explains the relatively weak MCT in that model. An analysis of the components of Fr shows that the inter-model relative standard deviations are respectively 14%, 13% and 5% for h, U and N, indicating that the variability in the Froude number, and thus the strength of the MCT in models, is dominated by the topography and the strength of the upstream wind.

The north–south profile of the topography of Madagascar and the vertical profiles of the mean zonal winds east of the island (between 52-60°E) are shown in Figs. 3 and 4. In general, models with low MCT tend to have either lower topography and stronger lower-level (below 800 hPa) zonal wind or high topography and relatively weak lower-level winds. For instance, the zonal wind intensity in GISS-E2-1G and BCC-ESM1 (two of the models with lowest MCT) is relatively weak while the mean topography is comparable to that of ERA5 and other models. For CESM2, which shows the weakest MCT, the maximum intensity in low level wind is well depicted but shifted towards the north compared to the observation. Similarly, for MIROC6, the low-level easterlies are extended too far north and less intense compared to ERA5. In contrast, GISS-E2-1H which has the lowest MCT

index reasonably depicts the observed values of Fr and its components, suggesting that the formation of the lee-side trough due to the dynamical adjustment of the easterlies is not fulfilled in this case. On the other hand, most models reasonably capture the observed upper-level easterly/ westerly circulation.

3.2 Link between MCT, monsoon winds and the Mascarene High

Barimalala et al. (2020) showed that during JFM, the NE monsoon penetrates farther into the northern Mozambique Channel, after which it curves toward northwestern Madagascar, reverses to northwesterly flow and feeds the circulation around the MCT. The analysis of the four monsoon indices defined in Sect. 2 shows that the simulations reasonably represent the zonal wind, flowing into mainland Africa over Tanzania (Fig. 5). In contrast, during JFM, 3 of the models (CESM2, GISS-E2-1-H and MIROC6) display easterlies over northern Mozambique Channel, instead of westerlies. These are due to the monsoon either becoming a westerly flow north of 10°S (GISS-E2-1-H) or it penetrating directly over the mainland without recurving to the east towards northern Madagascar. These 3 models are also characterized by weak MCT index compared to the ERA5 reanalysis. It is however not fully understood whether the erroneous wind direction leads to a weak MCT, or the weak low pressure affects the wind in the area. On the other hand, all models tend to overestimate the intensity of the southward meridional wind on both sides of the equator (Fig. 5).
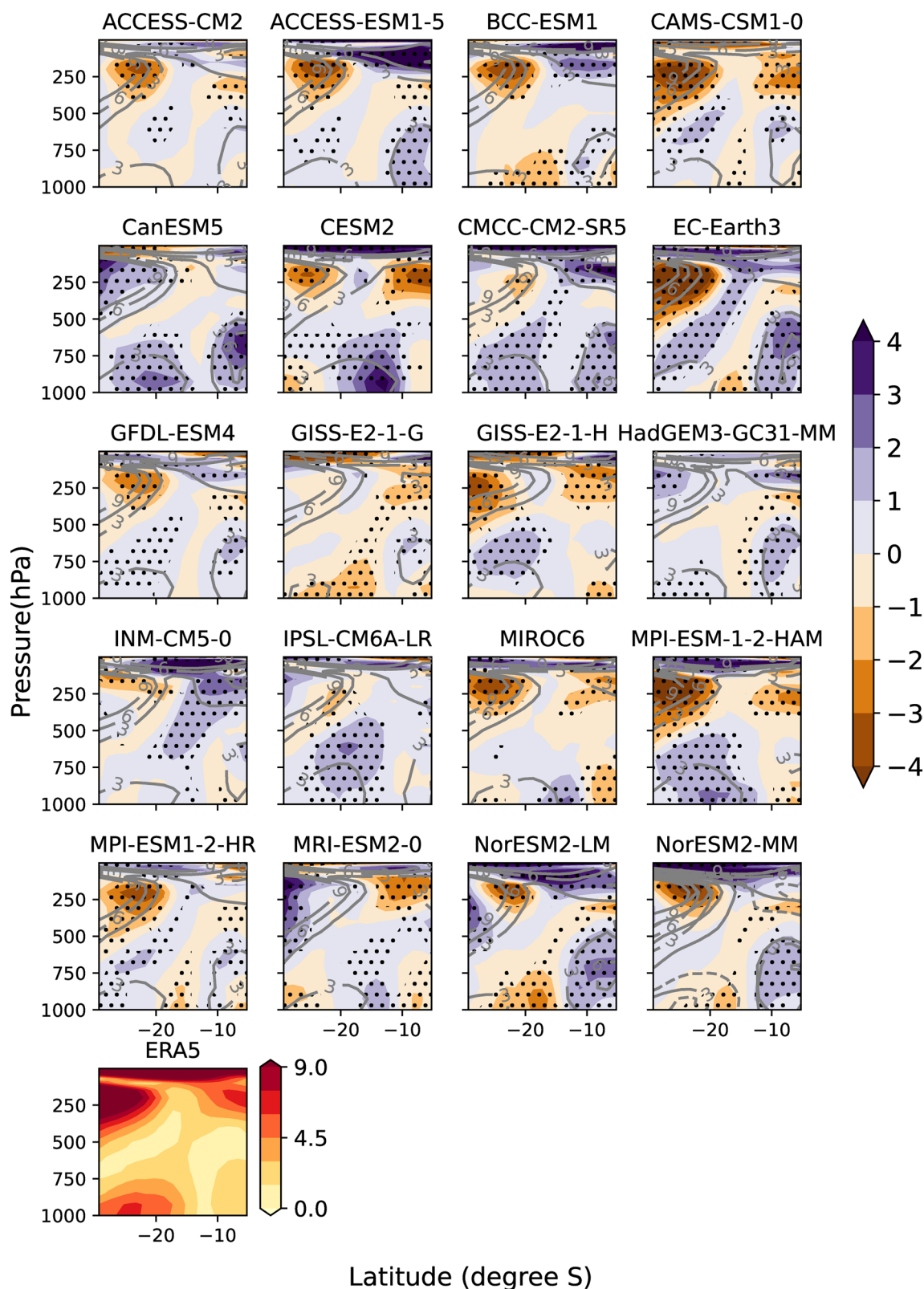
Fig. 4 Latitude-height vertical profile of the upstream zonal wind biases and the mean zonal wind (contours) over the east of Madagascar, averaged between 52-60°E the CMIP6 models and ERA5. Areas with statistically significant biases at 95% level are dotted. Units in m.s.$^{-1}$
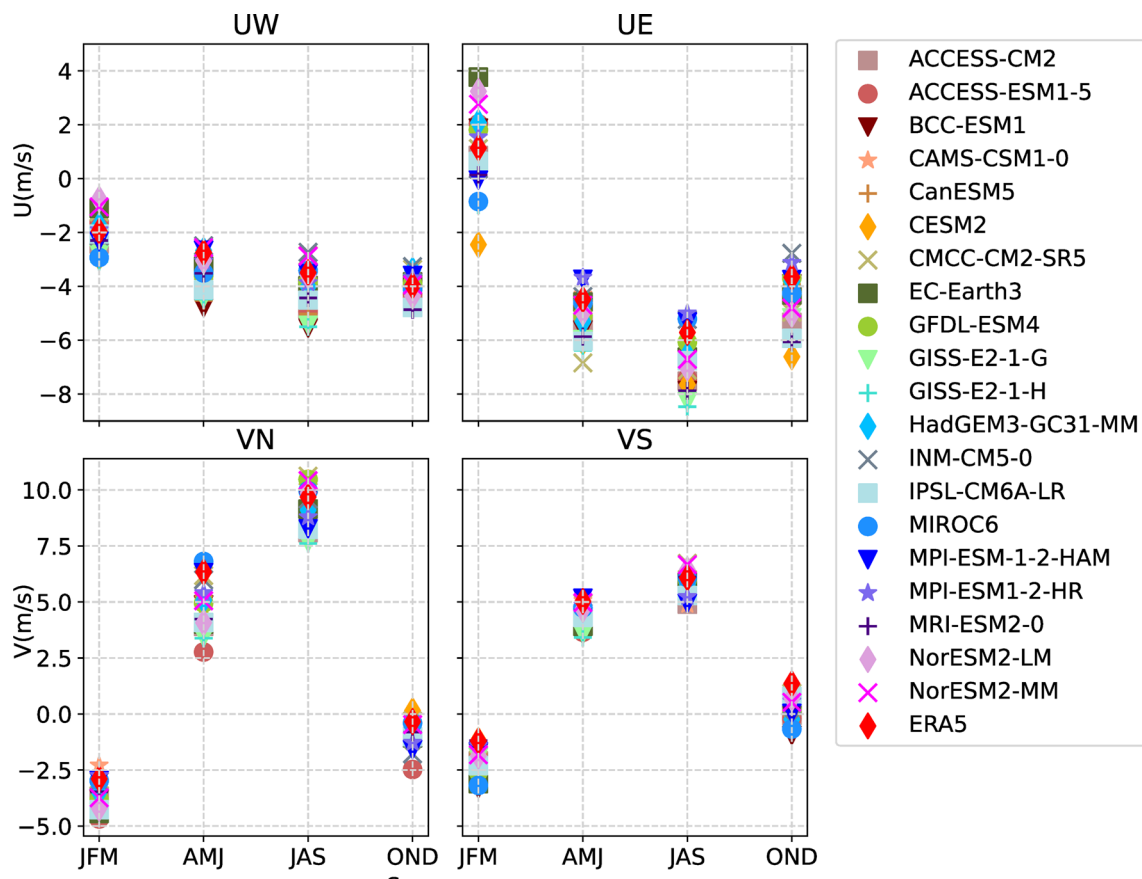
Fig. 5 Seasonal cycle of the northeasterly monsoon indices. UW—zonal wind penetrating into mainland, UE—zonal wind recurving toward Madagascar, VN—cross-equatorial northeasterly monsoon, and VS—meridional wind reaching the north of Madagascar. Units in m.s.$^{-1}$

Furthermore, the MCT is strongest when the MH is at its weakest intensity and located farther southeast over the South Indian Ocean basin (Barimalala et al. 2020). In that work, the MCT index is shown to be significantly correlated to the meridional shift of the northern border of the MH, such that the trough is stronger when the border is located more to the south, allowing the easterlies to flow over the topography of Madagascar and form the lee side vortex in the channel.

Overall, the CMIP6 models represent well the intensity of the MH during JFM, whereas there is a large spread in the location of the centers of this anticyclone (Figure S3), spanning from 33°S to 37°S. The two GISS models are among those with the southernmost centers, yet they show weak MCT indices. For other models, there is no clear link between the MCT and the MH, neither in the intensity nor in the location of the center.

Morioka et al. (2015) indicated that the location of the center of the MH does not fully reflect the zonal or meridional extent of the high pressure. Therefore, we investigated the northernmost and westernmost limits of the 1017-hPa

MSLP contour, which is essentially the lowest closed contour level around this high pressure system both in ERA5 and in the models.

The observed limits of the 1017-hPa MSLP are located around 14°S in the north and 40°E in the west. On the other hand, the northern limits in the models are too far south, ranging between 15–27°S whereas the western boundaries are located between 40–66°E (Fig. 6). Weak MH models tend to have their boundaries shifted farther southeast, with some of them (GISS-E2-1G, GISS-E2-1H, MIROC6) depicting a relatively weak MCT. These disagree with Barimalala et al. (2020), in which, by using reanalysis data, a weak MH located towards the southeastern part of the South Indian Ocean is associated with a strong MCT. A possible explanation is that the already weak MH in these models could be located too far to the southeast in the South Indian Ocean, leading to the associated easterlies being too weak to form the MCT (Fig. 4). For other models, there is no consistent association between the northern/western boundaries of MH and the strength of MCT.

Fig. 6 Mascarene High intensity (shading, in m), and location of the westernmost (northernmost) boundary of the 1017 hPa mean sea level pressure contour in x axis (y axis) around the Mascarene High area
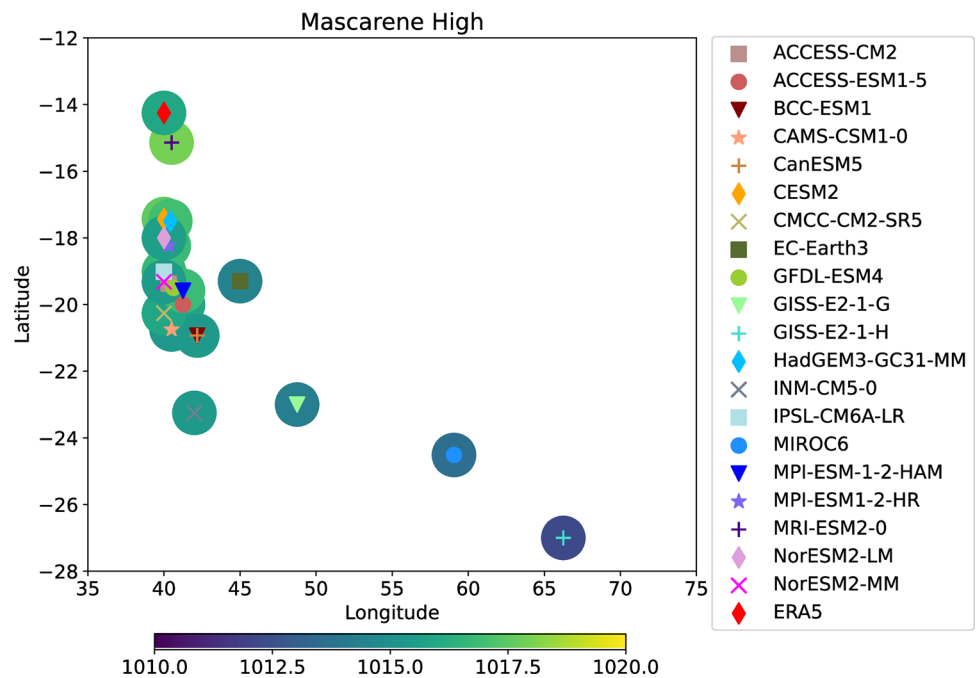
3.3 Mean behaviour of the vorticity over MCT area

The mean values, as well as the differences between the observed and simulated vorticity and divergence structure over the MCT are presented in Figs. 7 and 8. The figures show that the trough is extended to a deeper height, up to 400 hPa, associated with low-level convergence for models with strong MCT (e.g. EC-Earth, HadGEM3, NorESM2). It is also evident that models with weak MCT are characterized by not only a limited extension of the cyclonic vorticity into higher levels but also a weak low-level convergence (for BCC-ESM1) or low-level divergence (CESM2, GISS-E2-1G and GISS-E2-1H).

In the following, we analyze the different terms of the vorticity budget in the MCT area given by

$$\frac{\partial \zeta}{\partial t} + v.\nabla(\zeta + f) + (\zeta + f)\nabla_h.v_h - \hat{k}.(\frac{\partial v}{\partial p} \times \nabla \omega) - Residual = 0$$

$$\quad (1) \qquad\quad (2) \qquad\qquad (3) \qquad\qquad (4)$$

where ζ is the relative vorticity, v the 3D velocity, v_h horizontal velocity, ω vertical velocity, and f is the Coriolis parameter.

The different terms in the budget equations are:

(1) Vorticity tendency
(2) Advection term
(3) Horizontal divergence or stretching
(4) Twisting

Here, the individual terms are computed for each JFM between 1980–2014 and for every grid point, then averaged over time within the MCT area. The residual or friction term is obtained by the difference between the vorticity tendency and other terms to balance the budget.

The mean vertical structure of the different terms in the vorticity budget equation is displayed in Fig. 9. The vorticity tendency is relatively small (of the order of 10^{-16}) compared to other terms and is not shown on the figure. Below 600 hPa, the observed budget is dominated by a balance between the vertical advection and tilting terms as sources and the residual term as a sink. Between 200-600 hPa, the vertical advection becomes a sink, adding up to the residual term while these two terms are the main sources above 200 hPa.

On the other hand, the dominant terms in the CMIP6 models are somewhat different compared to ERA5 with the simulated magnitudes of the different vorticity budget components being relatively low. Below 800 hPa, the vorticity budget in the models is overall dominated by a balance between the stretching (source) and residual (sink) terms. An exception is seen in GISS-E2-1-H, GISS-E2-1-G and CESM2 models in which the budget sink is mainly from the residual and the source from the stretching term. Most models show a
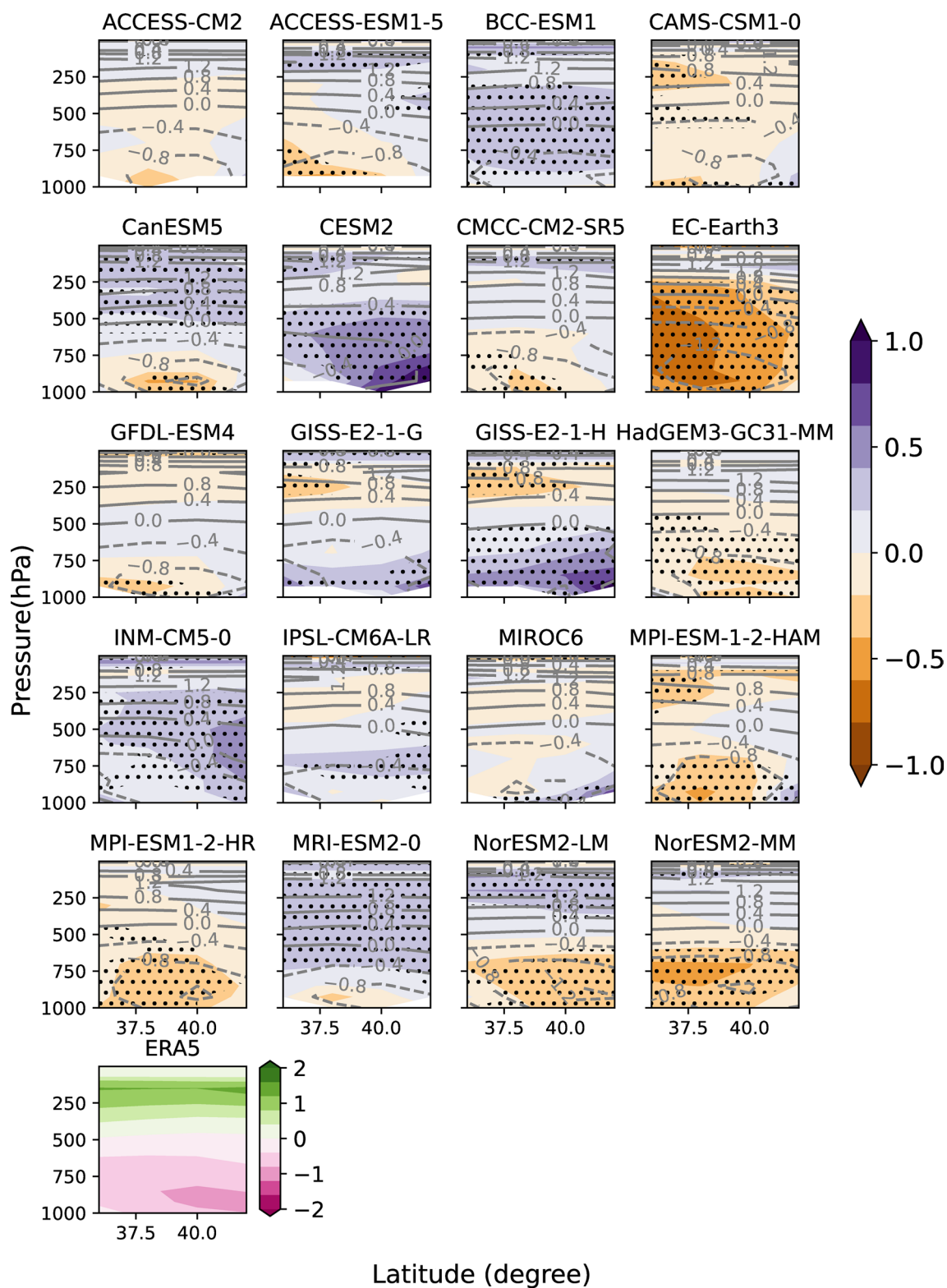
Fig. 7 Longitude-height profile of the relative vorticity biases (shaded) and the mean relative vorticity (contour) over the MCT area in the CMIP6 models and ERA5. Areas with statistically significant biases at 95% level are dotted. Units in.s.$^{-1}$
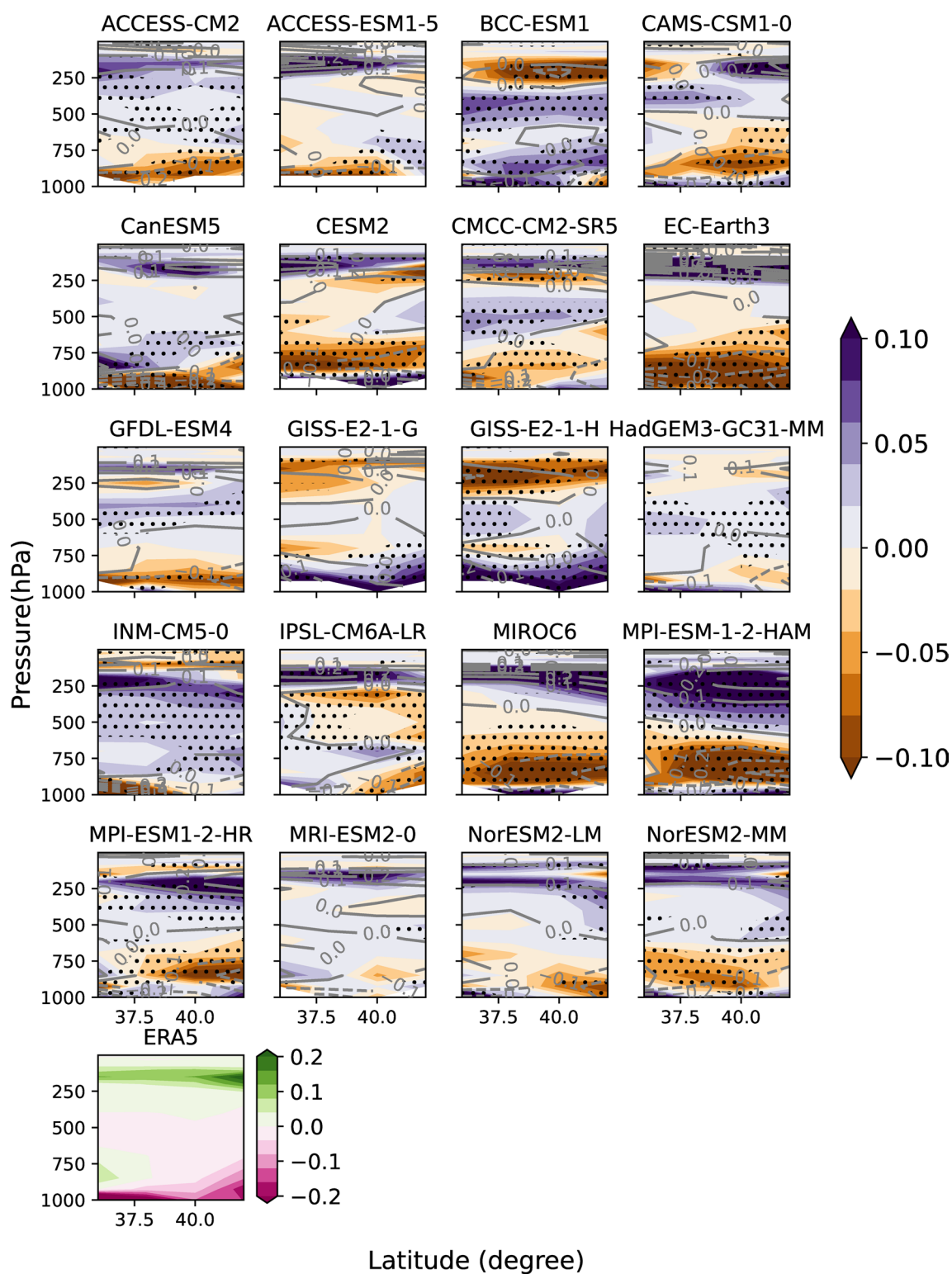
Fig. 8 Longitude-height profile of the divergence biases (shaded) and the mean divergence (contour) over the MCT area in the CMIP6 models and ERA5. Positive values are divergence and negative values convergence. Areas with statistically significant biases at 95% level are dotted. Units in.s.$^{-1}$
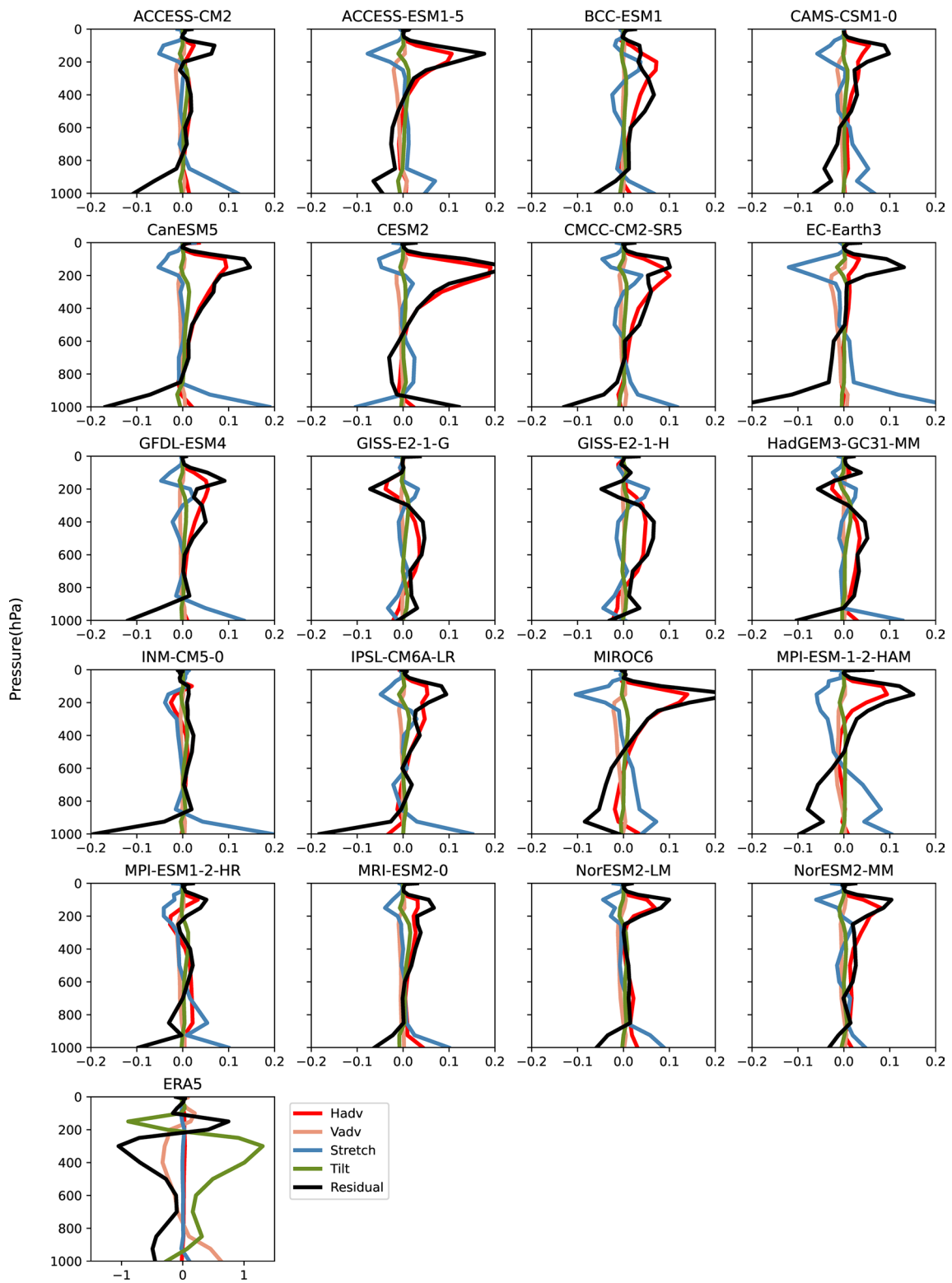
Fig. 9 Vertical profiles of the different terms in the vorticity budget over the MCT area in the CMIP6 models and ERA5
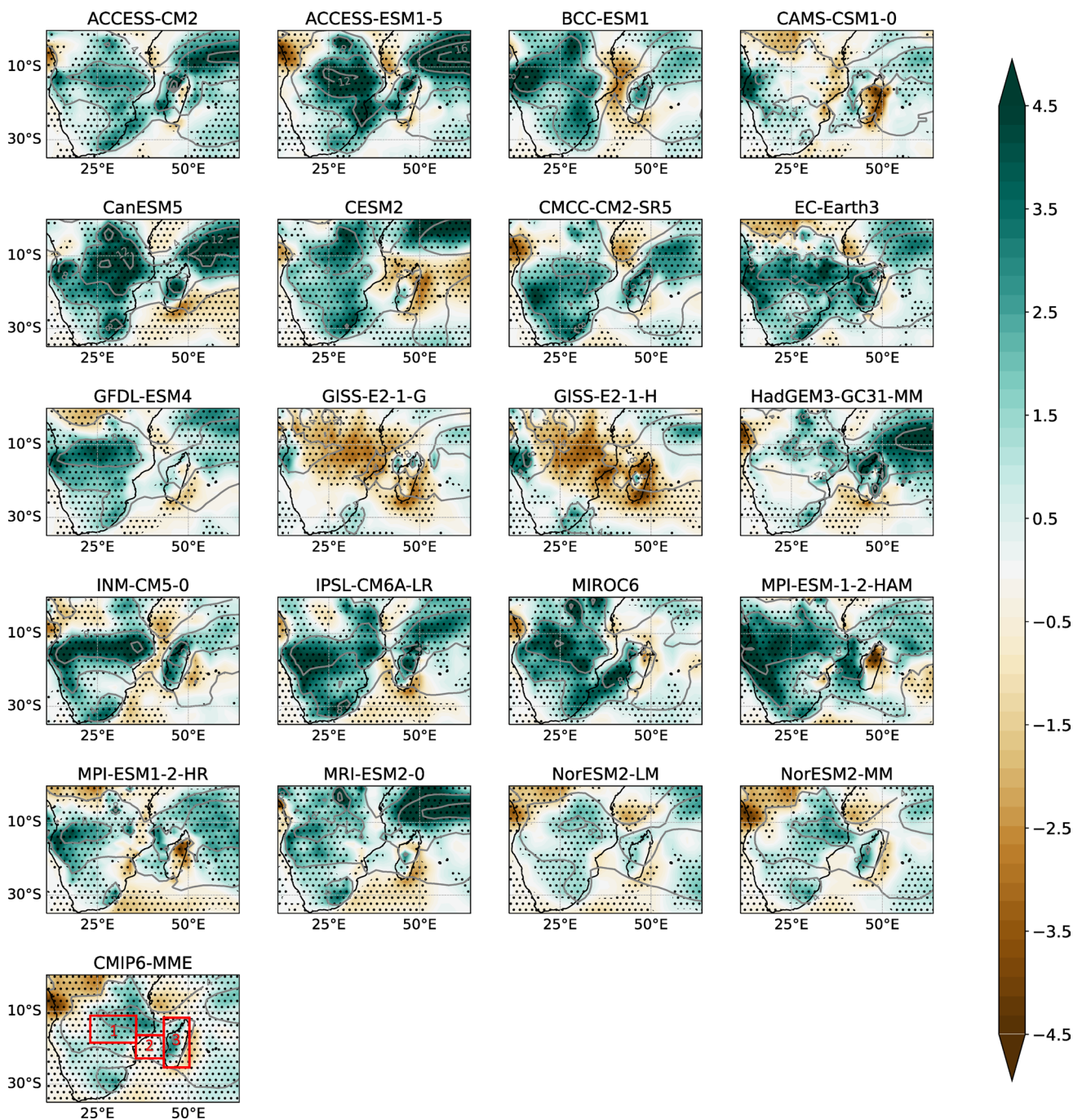
Fig. 10 Mean rainfall biases during JFM in the CMIP6 models and the ensemble mean. Boxes 1, 2 and 3 are used for the area average in Fig. 10. Box 1 corresponds to southern Africa, Box 2: Mozambique Channel and Box 3: Madagascar. Areas with statistically significant biases at 95% level are dotted Units mm.day.$^{-1}$

more complex balance of all the terms between 200-600 hPa. Above 200 hPa, the residual and horizontal advection become dominant as sources, while the stretching term is the main sink.

4 MCT and link with rainfall biases

Barimalala et al. (2018) showed that a weak MCT tends to increase summer rainfall over southern Africa and decrease

it over Madagascar. They suggested that a misrepresentation of the topography, and hence the MCT, could contribute to the dipole-like rainfall biases over southern Africa in state-of-the-art GCMs. In addition, observations of anomalous MCT summers (Barimalala et al. 2020) also showed the same rainfall patterns as the idealised WRF modelling study of (Barimalala et al. 2018). Pascale et al. (2019) also suggest a link between northerly moisture flux penetrating to the African mainland from the Indian Ocean and the strength of the MCT. They found that strong moisture bearing northerlies, which lead to excess rainfall over the mainland, are associated with a weak MCT.

Figure 10 presents the JFM rainfall biases in the CMIP6 models. An overall significant wet bias is displayed in the ensemble mean over the mainland south of 10°S, in the Mozambique Channel and over the western part of Madagascar. There is no apparent improvement in the CMIP6 rainfall biases over the southern African subcontinent compared to that of CMIP5, despite CMIP6 being a new round of model development with changes in the physics and increased resolution in some of the models. By looking at individual models, one common pattern is the significant excess in rainfall over most areas of the mainland, except in the two GISS models which show negative rainfall biases. In contrast, the bias pattern over the Mozambique Channel and Madagascar is highly model dependent. An area average of the rainfall biases calculated within three boxes over mainland southern Africa,

Mozambique Channel and Madagascar (Fig. 11) shows that about third of the models depict dry rainfall biases over Madagascar while all models (except the two GISS) display overall wet biases both over the Mozambique Channel and mainland.

A comparison of the MCT index bar graph (Fig. 2) and Fig. 11 shows no clear indication of the link between the strength of MCT and mean southern African rainfall in the models. For instance, EC-EARTH has the strongest MCT index among the models but also displays strong and significant wet biases over the whole subcontinent. On the other hand, the bias in the strength of MCT index is lowest in the ACCESS-ESM1-5, yet the model depicts large excess rainfall both over mainland and Madagascar. In addition, there is no significant correlation between the mean topography of Madagascar and rainfall in either of the three boxes.

A possible cause for the missing link is that the impact of MCT on southern African rainfall could be masked by other processes that drive the rainfall over the area. For instance, Munday and Washington (2017) found that the Angola Low is responsible for 40–60% of the total rainfall discrepancy in the models over southern Africa. The 850 hPa geopotential height maps in Fig. 12 show that most models are characterized by statistically significant stronger low pressure than ERA5 over the Angola low region, which could then lead to an overestimation of the rainfall over the subcontinent. However, such an assumption does not always hold given that models like MPI-ESM1-HR and MRI-ESM2-0

Fig. 11 Rainfall biases during JFM, averaged over the three boxes shown in Fig. 7. Box 1 corresponds to southern Africa, Box 2: Mozambique Channel and Box 3: Madagascar. Units mm.day.$^{-1}$
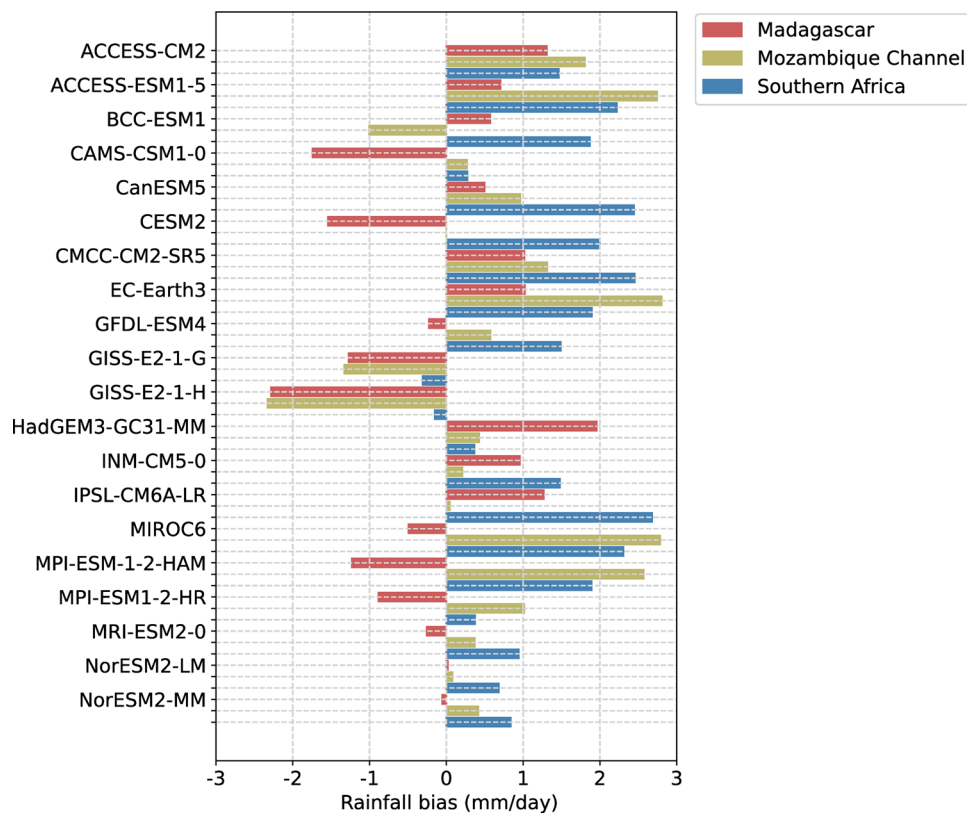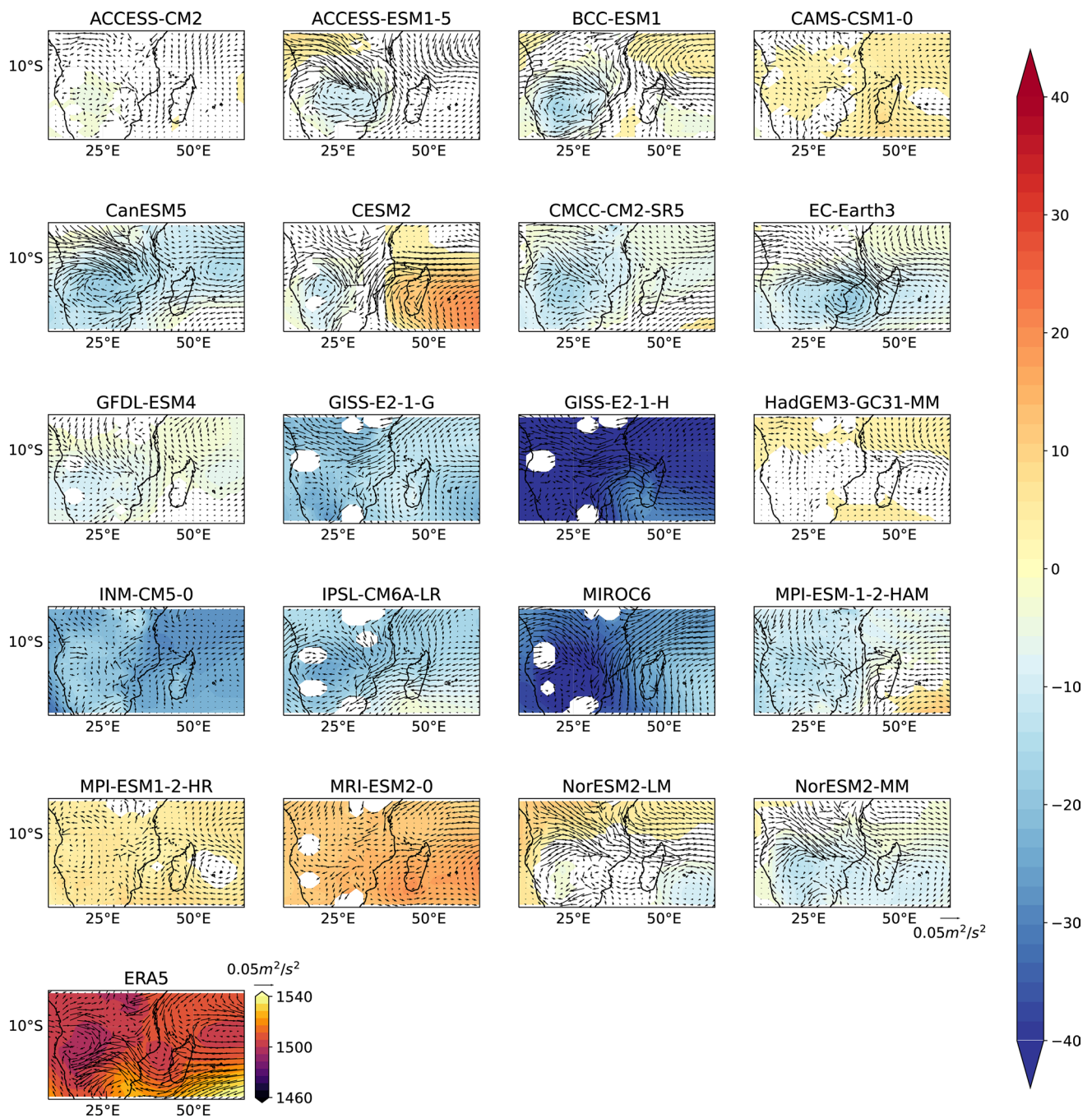
Fig. 12 Biases in moisture fluxes (arrows, in g.kg^{-1}.m.s^{-1}) and geopotential height (shading, in m) at 850 hPa during JFM in the CMIP6 models and ERA5

are characterized by weaker low pressure over the Angola/Namibia border but still overestimate the rainfall over the mainland.

Moreover, most models show an overall strong low level moisture flux originating from both the South Indian and South Atlantic Oceans (Fig. 12). The convergence of these fluxes over the mainland could lead to a strong SIOCZ, and thus excess rainfall there. These patterns are similar to that

of the CMIP5 low level moisture fluxes in Lazenby et al. (2016). In the two GISS models, although the MCT is relatively weak, the penetration of the moisture flux from the tropical Atlantic is underestimated leading to weak low level convergence and a deficit in rainfall over southern Africa.

Differences in vertical velocity between ERA5 and the CMIP6 models, averaged over 20-60°E and 15-26°S during JFM are shown in Fig. 13. The latitude range includes the
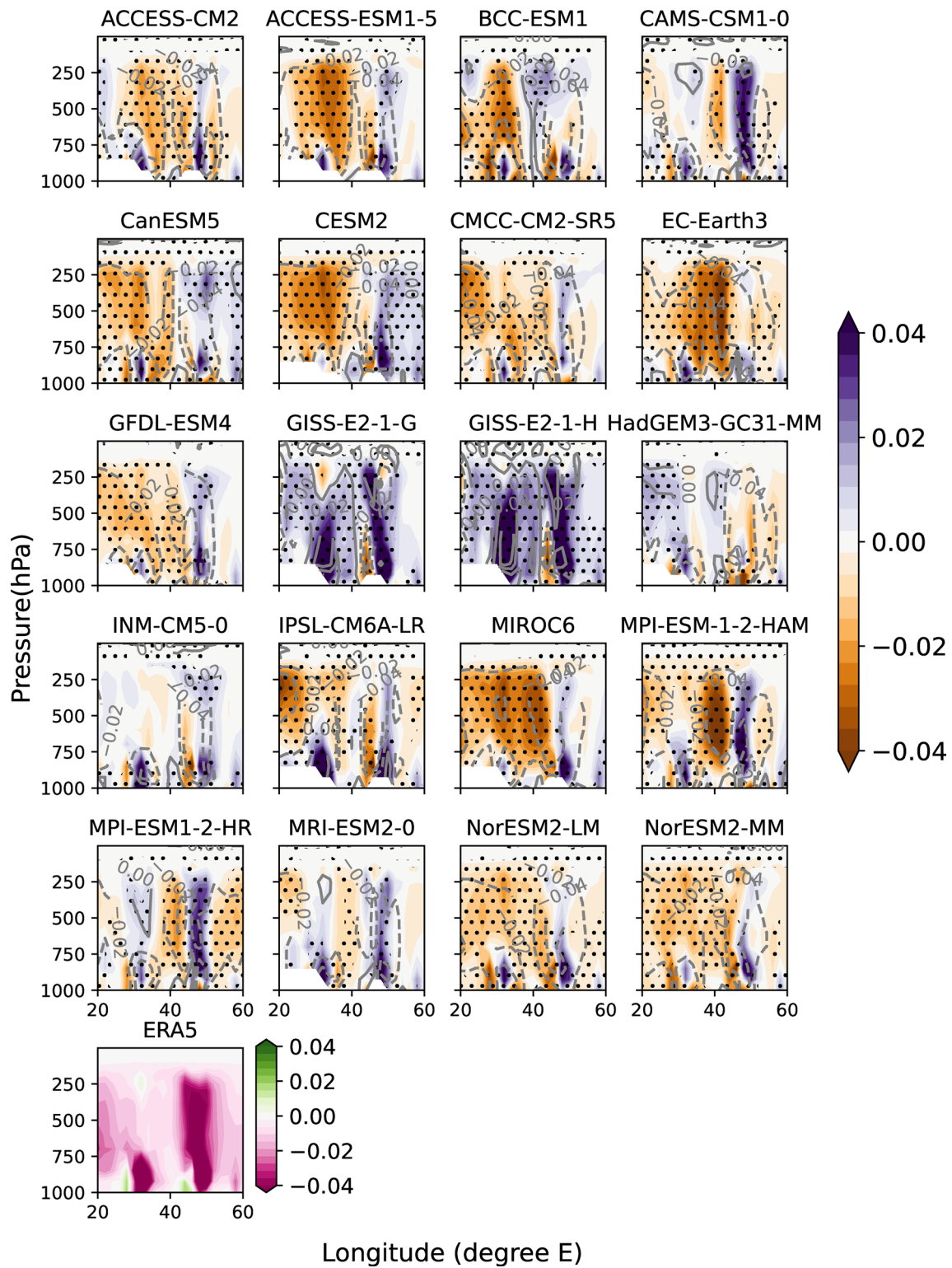
Fig. 13 Longitude-height profile of omega biases (shaded) and the mean omega (contour) between 15-26°S. Positive values represent sinking air and uplift for negative values. Areas with statistically significant biases at 95% level are dotted. Units in Pa

central and southern parts of the Mozambique Channel, covering the location of the MCT in ERA5 and the models. In the reanalysis, the whole area is characterized by upward motion (negative values), with much weaker intensity over the Mozambique Channel (around 40°E) and deep convection up to 200 hPa extending over the Angola Low region on the mainland (20-25°E) and in the east over Madagascar (around 48-50°E). In addition, there is a shallow convection cell over the low-lying regions of northeastern South Africa and Mozambique, between 30-35°E. In contrast, most models show a low-level subsidence (below 800 hPa) and overestimated convection at higher levels in the Mozambique Channel. Significantly strong upward motions compared to ERA5 are also displayed on both sides of the channel, which could potentially counteract the impacts of the MCT on regional rainfall. The diabatic heating associated with the strong convection in the models could enhance the large scale moisture inflow, influence the characteristics of the regional overturning circulation (Chang and Nigam 2009) and thus disrupt the MCT-rainfall link.

5 Summary and conclusions

In this work, we investigated how state-of-the-art coupled climate models from CMIP6 represent the Mozambique Channel Trough and its link to southern African rainfall. The ensemble mean reasonably captures the observed strength of the MCT despite the large spread among the individual models. By excluding the two GISS models which show unrealistically weak MCT, the strength of the trough is significantly correlated with the non-dimensional Froude number. This confirms the role played by the topographical adjustment of the easterlies in the formation of the trough. For strong MCT models, the cyclonic circulation that characterizes the trough is extended deeper in the atmosphere and associated with low level convergence. On the other hand, weak MCT models tend to have either weak low-level convergence compared to the reanalysis or low-level divergence. Some of the weak MCT models are also associated with incorrect wind directions over the northern Mozambique Channel.

The analysis of the vorticity budget shows that the simulated vorticity tendency is mainly dominated by a balance between the stretching and residual terms. The stretching dominance is explained by the conservation of potential vorticity while passing over the topography of Madagascar. In contrast, the vorticity tendency is driven by vertical advection, tilting and residual terms in the reanalysis. These results are in agreement with Barimalala et al. (2020) which shows the same dominant terms in a composite of strong MCT years, suggesting a strong influence of local forcing on the trough.

This study also shows an overall statistically significant excess in model rainfall over the southern African mainland and Mozambique Channel, whereas a mixed signal is seen over Madagascar. The CMIP6 models do not appear to improve the rainfall biases that have persisted through different CMIP generations over the subcontinent. The link between MCT and rainfall is not present in the models. This could be because the impacts of the MCT on rainfall are masked by the misrepresentation of other key processes such as the Angola Low and the low level moisture flux over southern Africa which are relatively strong in most models. In addition, compared to the ERA5 reanalysis, the models show strong convection over the mainland, the Mozambique Channel and Madagascar which could lead to excessive rainfall in these areas.

Although this study is not meant to analyze the source of the rainfall biases over southern Africa in the CMIP6 models, these results show the complexity of the mix of processes that drive the rainfall in the area. An analysis of these individual processes as well as the link between them is suggested to advance our understanding of the source of errors and uncertainties in the CMIP6 models.

Declarations

References

Adler RF et al (2003) The version-2 global precipitation climatology project (GPCP) monthly precipitation analysis (1979–present). J Hydrometeorol 4(6):1147–1167. https://doi.org/10.1175/1525-7541(2003)004%3c1147:TVGPCP%3e2.0.CO;2

Barimalala R, Desbiolles F, Blamey RC, Reason CJC (2018) Madagascar Influence on the South Indian Ocean convergence zone, the Mozambique channel trough and southern African rainfall. Geophys Res Lett 45:11380–11389. https://doi.org/10.1029/2018GL079964

Barimalala R, Blamey RC, Desbiolles F, Reason CJ (2020) Variability in the Mozambique channel trough and impacts on southeast African rainfall. J Clim 33:749–765

Chan SC, Nigam S (2009) Residual diagnosis of diabatic heating from ERA-40 and NCEP reanalyses: intercomparisons with TRMM. J Clim 22:414–428. https://doi.org/10.1175/2008JCLI2417.1

Christensen JH et al (2007) Regional climate projections. In: Solomon S et al (eds) Climate change 2007: the physical science basis. Cambridge University Press, pp 847–940

Dieppois B, Rouault M, New M (2015) The impact of ENSO on Southern African rainfall in CMIP5 ocean atmosphere coupled climate models. Clim Dyn 45:2425–2442. https://doi.org/10.1007/s00382-015-2480-x

Dieppois B, Pohl B, Crétat, et al (2019) Southern African summer-rainfall variability, and its teleconnections, on interannual to interdecadal timescales in CMIP5 models. Clim Dyn 53:3505–3527. https://doi.org/10.1007/s00382-019-04720-5

Engelbrecht FA, McGregor JL, Engelbrecht CJ (2009) Dynamics of the conformal-cubic atmospheric model projected climate-change signal over southern Africa. Int J Climatol 29:1013–1033

Eyring V, Bony S, Meehl GA, Senior CA, Stevens B, Stouffer RJ, Taylor KE (2016) Overview of the coupled model intercomparison project phase 6 (CMIP6) experimental design and organization. Geosci Model Dev 9:1937–1958. https://doi.org/10.5194/gmd-9-1937-2016

Gleckler PJ, Taylor KE, Doutriaux C (2008) Performance metrics for climate models. J Geophys Res 113:D06104. https://doi.org/10.1029/2007JD008972

Hart NCG, Reason CJC, Fauchereau N (2010) Tropical-extratropical interactions over southern Africa: three cases of heavy summer season rainfall. Mon Weather Rev 138(7):2608–2623. https://doi.org/10.1175/2010MWR3070.1

Hart NCG, Reason CJC, Fauchereau N (2013) Cloud bands over southern Africa: seasonality, contribution to rainfall variability and modulation by the MJO. Clim Dyn 41(5–6):1199–1212. https://doi.org/10.1007/s00382-012-1589-4

Hersbach H, Bell B, Berrisford P et al (2020) The ERA5 global reanalysis. QJR Meteorol Soc 146:1999–2049. https://doi.org/10.1002/qj.3803

James R et al (2018) Evaluating climate models with an African lens. Bull Amer Meteor Soc 99:313–336. https://doi.org/10.1175/BAMS-D-16-0090.1

James R, Hart NCG, Munday C, Reason CJC, Washington R (2020) Coupled climate model simulation of tropical–extratropical cloud bands over southern Africa. J Clim. https://doi.org/10.1175/JCLI-D-19-0731.s1

Lazenby M, Todd M, Wang Y (2016) Climate model simulation of the South Indian Ocean convergence zone: mean state and variability. Climate Res 68:59–71. https://doi.org/10.3354/cr01382

Morioka Y, Takaya K, Behera SK, Masumoto Y (2015) Local SST impacts on the summertime Mascarene high variability. J Climate 28:678–694. https://doi.org/10.1175/JCLI-D-14-00133.1

Munday C, Washington R (2017) Circulation controls on southern African precipitation in coupled models: the role of the Angola low. J Geophys Res Atmos 122:861–877. https://doi.org/10.1002/2016JD025736

Munday C, Washington R (2018) Systematic climate model rainfall biases over southern Africa: links to moisture circulation and topography. J Climate 31:7533–7548. https://doi.org/10.1175/JCLI-D-18-0008.1

Munday C, Washington R (2019) Controls on the diversity in climate model projections of early summer drying over southern Africa. J Climate 32(3707):3725. https://doi.org/10.1175/JCLI-D-18-0463.1

Pascale S, Pohl B, Kapnick S, Zhang H (2019) On the Angola low interannual variability and its role in modulating ENSO effects in southern Africa. J Climate 32:4783–4803. https://doi.org/10.1175/JCLI-D-18-0745.1

Schaller N, Mahlstein I, Cermak J, Knutti R (2011) Analyzing precipitation projections: a comparison of different approaches to climate model evaluation. J Geophys Res 116:D10118. https://doi.org/10.1029/2010JD014963

Smolarkiewicz PK, Rotunno R (1989) Low Froude number flow past three-dimensional obstacles. Part I: baroclinically generated lee vortices. J Atmos Sci 46(8):1154–1164

Sushama L, Laprise R, Caya D, Frigon A, Slivitzky M (2006) Canadian RCM projected climate-change signal and its sensitivity to model errors. Int J Climatol 26:2141–2159